J Solid State Electrochem (2007) 11:1013–1021
DOI 10.1007/s10008-007-0262-z

ORIGINAL PAPER

Surface reactivity of polypyrrole/iron-oxide nanoparticles: electrochemical and CS-AFM investigations

A. Pailleret · N. T. L. Hien · D. T. M. Thanh · C. Deslouis

Received: 10 October 2006 / Revised: 14 December 2006 / Accepted: 15 December 2006 / Published online: 1 February 2007

Abstract Composite materials based on iron-oxide nanoparticles (magnetite, hematite, and maghemite) and tetraoxalate-doped polypyrrole (PPy) were electrochemically generated from aqueous solutions. Their composition was determined using electrochemical quartz crystal microbalance experiments. The oxide percentage in mass was found to vary from 17 to 27% depending on the oxide identity. They were all shown to be fascinating candidates as protective materials against corrosion of iron and carbon steel materials although maghemite-nanoparticle-loaded polypyrrole films offer the best performances. An anionic surfactant (sodium dodecylsulfate) was added to the electrodeposition solution to avoid the formation of clusters. These anions were also shown to improve the conductivity of the resulting PPy films, while the presence of oxide nanoparticles tends to decrease this same surface conductivity. On the other hand, the correlation between the morphology and the local conductivity appears to be more obvious in the absence of anionic surfactants than in their presence. This aspect is discussed although it still needs further investigation.

Keywords Polypyrrole · Iron-oxide nanoparticles · Composite materials · CS-AFM · Corrosion

Contribution to the International Workshop on Electrochemistry of Electroactive Materials (WEEM-2006), Repino, Russia, 24–29 June 2006.

A. Pailleret · C. Deslouis (✉)
UPR 15 CNRS—LISE, Université Pierre et Marie Curie,
4 place Jussieu,
75252 Paris Cedex 05, France
e-mail: cld@ccr.jussieu.fr

N. T. L. Hien · D. T. M. Thanh
Institute of Tropical Technology, VAST,
18 Hoang Quoc Viet, Cau Giay,
Hanoi, Vietnam

Introduction

Composites based on conducting polymers and metallic oxides raise a growing interest for their potential applications in several domains such as protection against corrosion, electrocatalysis, or as electrode materials for batteries. The properties which govern their performances can be related either to bulk or interfacial characteristics, the former being possibly reflected in the latter ones.

Protection mechanism by polypyrrole (PPy) films used as protective coatings against corrosion of iron or carbon steel in chloride solutions has been demonstrated to be of the anodic galvanic type, and the main cause of the loss of protection was shown to be the progressive invasion of the film by chloride ions [1]. It was shown in particular that this protective power could be increased either by changing the ionic selectivity of the film [2], thus improving the barrier effect with respect to aggressive anions (e.g., chlorides), or by synthesizing electrochemically PPy/oxide composites that enhance the oxidizing properties of the film. It was demonstrated that the presence of iron-oxide microparticles, in particular Fe_3O_4, in the PPy matrix yielded optimized protection by extending the protection time [3].

As these iron oxides display in general a rather low conductivity and therefore a low ability to transfer the charge necessary for keeping the metal passivation, the possibility of using nanoparticles instead of microparticles was explored in this study so as to allow a maximum oxidizing capacity for a given amount of these materials.

In this work, different iron oxides (Fe_3O_4, α-Fe_2O_3, and γ-Fe_2O_3) have been incorporated during the electrodeposition of PPy films on iron electrodes in electrolytes containing pyrrole (Py) monomer and some or all of the following compounds: tetraoxalate anion, sodium dodecylsulfate, and

iron oxides in suspension. The maximum amounts of particles that can be inserted and their oxidative power are parameters of relevance in this application. The resulting films have been therefore characterized by electrochemical quartz crystal microbalance (EQCM). The evolution of the open-circuit potential (OCP) for the resulting coated iron electrodes has been monitored in 3% NaCl solutions.

The surface reactivity which is also a relevant parameter of the film properties cannot be directly assessed except with the scanning electrochemical microscopy technique, but the measurement volume is still at least of the order of the tip size which means not smaller than 1 μm or a few micrometers.

It was therefore decided to combine atomic force microscopy (AFM) to allow a morphological characterization at the nanometer scale in ex situ conditions and the current-sensing AFM (CS-AFM) which senses the local and superficial electronic conductivity of a material. Measuring the surface electronic conductivity in dry conditions may lead to relations existing between this surface conductivity distribution, the surface reactivity, and the material morphology. It may thus allow improving the growth mechanism so as to reach better performances for these films. Recent combined use of AFM and CS-AFM on polypyrrole films has been reported to investigate the influence of parameters such as thickness [4], aging and doping effects [5], or counterion influence [6] of the PPy films on their surface conductivity. More generally speaking, this combination of modes of AFM was also applied for other conducting polymers such as polythiophene [7, 8], polyaniline alone [9–11], or blended in an insulating poly(methyl methacrylate) matrix [12], as well as for other types of materials such as boron-doped diamond-type materials for example [13–15].

Experimental conditions

AFM and CS-AFM observations were carried out in air using a molecular imaging instrument in the contact mode. This latter instrument was composed of a Pico-LE base equipped with a micropositioning device aimed at the precise positioning of the AFM tip in the x–y plane of the sample, a large zone scanner (100×100 μm) bearing a photo detector, and the AFM nose adequate for CS-AFM experiments. A PicoScan 2100 controller connected to a computer was used to drive the scanner and to collect the data generated by the laser impact on the photo detector. In this purpose, conducting AFM probes made from rectangular silicon cantilevers bearing conical silicon tips coated with a Pt–Ir thin film were used. The curvature radius at their apex is 35 nm in average, and their spring constant was within the range of 0.6–6 N m^{-1} with a typical value close to 2 N m^{-1}. The loading force on the cantilever was maintained to zero. This value was chosen so as to spare the surface of the composite materials investigated in this work. Three images were successively made at the same spot to ensure that neither the AFM tip nor the samples were damaged. This procedure was repeated using three different zones per sample and two samples for each given set of growth conditions. With the help of this rather heavy procedure, it was concluded that our topography and local current images were never altered by any kind of variations from a sample to another. In other words, a very satisfying reproducibility was observed for our images. Let us emphasize also that all AFM images shown hereafter, whether they are topography or conductivity images, underwent a plane correction process.

The electrochemical setup consisted of an electrochemical interface AUTOLAB PGSTAT 30 (from Eco Chemie). Electrosyntheses were carried in galvanostatic conditions (1 mA/cm^2) at room temperature (θ=25±0.1 °C) with a three-electrode cell arrangement, a platinum grid as counter electrode, and a saturated sulfate reference electrode (SSE). The pyrrole was preliminary distilled. After the coating synthesis, the samples were rinsed in demineralized water and then dipped at open circuit in a 3% NaCl aqueous solution used as a corrosive medium.

The electropolymerization solution was composed of potassium tetraoxalate (PTO, 0.05 M, pH~1.8), pyrrole (0.1 M), sodium dodecylsulfate ($C_{12}H_{23}SO_4Na$ or SDS, 10^{-4} M), and iron-oxide nanoparticles [the same amount per unit volume (1 g l^{-1}) was used for all oxides]. α-Fe_2O_3 (hematite) and Fe_3O_4 (magnetite) were provided from Sigma-Aldrich, and γ-Fe_2O_3 (maghemite) was prepared by calcination of nitrates and grinding.

Substrates for AFM or CS-AFM observations were prepared by depositing 45-nm-thick platinum disks (diameter=4 mm) on mica substrates using the magnetron sputtering technique. The roughness measured by AFM was found to be below 1 nm for naked mica and platinum disk electrodes deposited on mica. The resulting smooth platinum disks were then used as working electrodes. In this case, the duration of the electrodeposition step of our PPy/iron-oxide composite films was 100 s (1 mA/cm^2 or 0.1 C/cm^2), which corresponds to an approximate thickness δ of 170 nm according to the following formula [16]:

$$\delta = \frac{Q(M_m + y.M_A)\eta}{(2+y)FA\rho} \quad (1)$$

In this equation, Q is the coulombic charge used for the electrodeposition process, M_m is the molar mass of the pyrrole monomer (67 g mol^{-1}), M_A is the molar mass of the doping anion (89 g mol^{-1}), y is the doping rate (0.33), ρ is the density of polypyrrole films (1.5 g cm^{-3} [16]), η is the electrodeposition rate (60%), and A is the geometrical area of the electrode (0.126 cm^2).

Substrates for corrosion tests (OCP) were iron rods (diameter 5 mm) from Goodfellow (99.99% pure), which were coated with an insulating cataphoretic lacquer and subsequently embedded in an epoxy resin. Before the electrosynthesis, the cross section of the rod was polished using an emery paper down to the 2,400-grit size, rinsed with demineralized water, and finally dried in pulsed warm air. The electrosynthesis duration was 2,000 s (1 mA/cm^2 or 2 C/cm^2) corresponding to an approximate thickness of 3.43 μm according to Eq. 1.

Corrosion tests were performed by following the time evolution of the OCP with respect to a saturated calomel reference electrode. For better comparison, all further potentials have been referred to an SSE.

For EQCM measurements, two gold electrodes were deposited on the opposite faces of the quartz crystal (CQE, Troyes, France): They allowed electric connections to an oscillator circuit, whereas the electrode exposed to solution was used as the working electrode in a usual three-electrode electrochemical setup and connected to a Sotelem potentiostat.

Preliminary observations of the nanoparticles were conducted using a 100-kV Jeol transmission electron microscope (TEM).

Experimental results

TEM observations

TEM observations displayed in Fig. 1 show the morphology of the nanoparticles for the three iron oxides used in this work. Maghemite (γ-Fe_2O_3) and hematite (α-Fe_2O_3) present rather uneven shapes with a mean size around 10 nm. Magnetite (Fe_3O_4) conversely has a more spherical aspect with larger sizes around 30 nm. However, as the iron-oxide nanoparticles are prone to form clusters in solution, dodecylsulfate (DS) anions were used to minimize this effect. In fact, for all the investigated oxides, the isoelectric point, used to represent the pH at which an immersed solid oxide surface has a zero net charge, is around 6–8 [17]. For lower pH, which is the case in our experiments, the oxide surface becomes then positively charged. It is thus predictable that an anionic surfactant such as DS, when added to the electrolytic solution, will adsorb on the iron-oxide nanoparticles by its polar head, the hydrophobic tail being oriented toward the solution and thus preventing particle aggregation.

As it was shown earlier that DS anions can be used efficiently for corrosion protection as counterion for PPy synthesis [18], it was verified in this study with a DS-specific electrode that free DS concentration in solution, in the presence of the nanoparticles (1 g l^{-1}), was less than 10^{-6} M when the initial SDS concentration was 10^{-4} M. This was consistent with the huge specific area of the nanoparticles in the range of 100 m^2 g^{-1}. Such a low DS concentration was proved [18] to be inefficient with respect to corrosion protection.

EQCM experiments

The mass increase of PPy films with time (see Fig. 2) is linear for all conditions with or without nanoparticles as shown by EQCM measurements during the electrochemical synthesis of the composite materials. As the film thickness remains lower than 150 nm, the behavior of the film is ideally elastic and the Sauerbrey equation applies. It can be inferred that the films are homogeneous, and the particle distribution is rather uniform. The slopes in Fig. 2 are higher for the composite films. From the slopes in Fig. 2, the oxide content in the film can be determined. In this purpose, the oxide percentage in mass was first calculated by using the formula:

$$\%\,\text{oxide in mass} = (\text{mass of the composite film} - \text{mass of the PPy/PTO/DS film})/\text{mass of the composite film}.$$

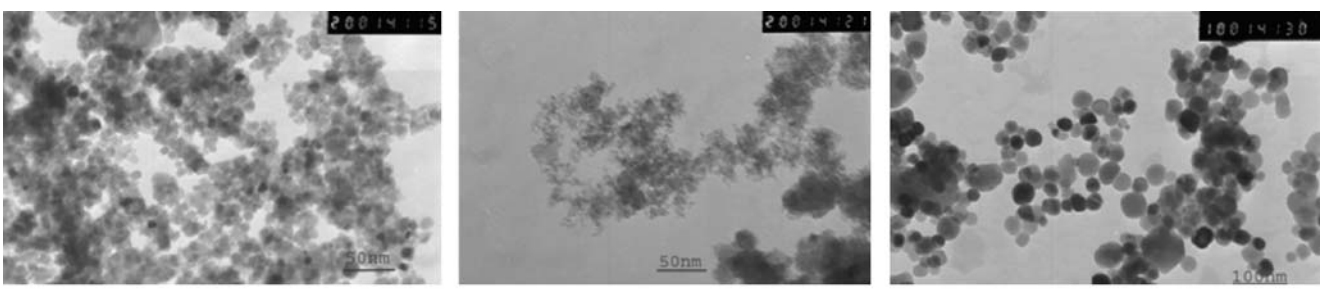

a b c

Fig. 1 Transmission electronic microscope photographs of **a** maghemite (γ-Fe_2O_3), **b** hematite (α-Fe_2O_3), and **c** magnetite (Fe_3O_4)

All the masses used in this formula obviously correspond to the films electrodeposited using the same experimental conditions (see Fig. 2). As a consequence, the percentage of oxide in volume was deduced by using the formula:

$$\%\,\text{oxide in volume} = (\text{mass of the incorporated oxide nanoparticles} \times \text{average density of PPy films}) / (\text{oxide density} \times \text{mass of the PPy/PTO/DS film}).$$

The value of the average density of PPy films used for this calculation was 1,500 kg/m^3 [16]. The resulting values reported in Table 1 for each of the three oxide types indicate that magnetite is the more concentrated type of nanoparticles in the film.

The protection efficiency as indicated by the OCP (see Fig. 3) is significantly improved in the presence of the oxides: the potential plateau around −0.3 V/SSE corresponds to passivity conditions for which the metal is protected. This result is consistent with the conclusions given in the paper of Garcia et al. [3] with respect to the relative efficiencies of magnetite and hematite. In addition, it shows a significant increase of the protection time with maghemite. A comparison can be done as the same charge was used for the films synthesized in the work of Garcia et al. [3]: the percentages in mass for the different oxides were similar for hematite in the study of Garcia et al. [3] (about 20%) as compared to 17% for maghemite and 24% for hematite in this study. Conversely, the incorporated amount of magnetite in this study (~27%) is significantly higher than in the work of Garcia et al. [3] (~14%).

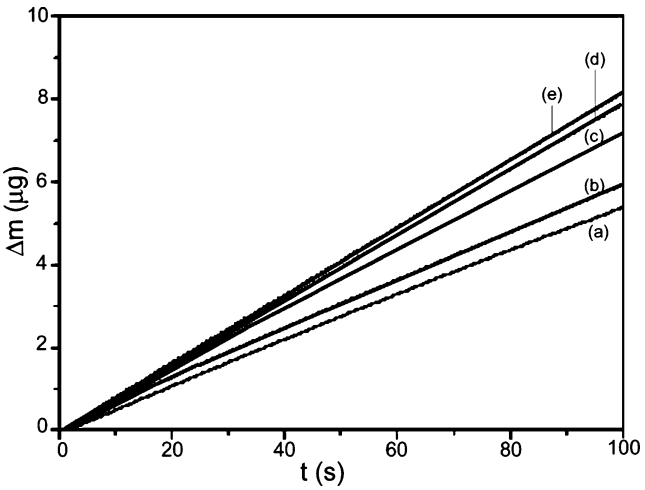

Fig. 2 Electrochemical quartz crystal microbalance measurements: mass increase (μg) with time (s) for different solutions: **a** pyrrole (0.1 M)+potassium tetraoxalate (0.05 M), **b** Py+PTO+DS (10^{-4} M), **c** Py+PTO+DS+γ-Fe_2O_3, **d** Py+PTO+DS+α-Fe_2O_3, **e** Py+PTO+DS+Fe_3O_4. Syntheses charge 0.1 C cm^{-2}. The concentration of all oxide suspensions is 1 g l^{-1}

CS-AFM experiments

The AFM and CS-AFM images are reported in Figs. 4, 5, and 6. The rms roughness average value is less than 10 nm as compared to the common thickness of the films of 170 nm. The characteristics of the "reference film" synthesized only with PTO as counterion are shown in Fig. 4. The topography image (Fig. 4a) displays a globular aspect with protrusions appearing as white features of average size in the *x*–*y* plane in the order of 200 nm. The surface conductivity image is represented in Fig. 4b. The potential imposed to the substrate with respect to the tip was negative in the present case and, therefore, the more conductive parts of the image correspond to more negative currents (black areas in the image) and more insulating ones to low or zero currents (white areas, respectively). In Fig. 4c, a typical variation of the current is shown along a scan line. The combination of all these scan lines is used for producing images such as Fig. 4b.

The question of a clear correlation between the morphology and the conductivity images is not straightforward. However, a sound conclusion could have been drawn only on the basis of a mathematical space correlation performed between the two images, but this could not be done in this study because of the domains where the current signal is saturated (as observed in scan lines such as the one in Fig. 4c). The main result is that the conductivity image is dominated by white areas, which indicates a rather low conductivity of the PPy film. This is consistent with the fact that oxalate is not a very efficient doping ion for PPy. The choice of this counterion was rather done on the basis of the possibility it offers to find a single common potential for

Table 1 Resulting values of the different types of films

Films	Slope (μg/s)	Oxide in mass (%)	Oxide in volume (%)
PPy/oxalate	0.05426	–	–
PPy/oxalate+DS	0.05963	–	–
PPy/oxalate+DS+γ-Fe_2O_3	0.07191	17.08	5.5
PPy/oxalate+DS+α-Fe_2O_3	0.07843	23.97	8.3
PPy/oxalate+DS+Fe_3O_4	0.08150	26.83	10.0

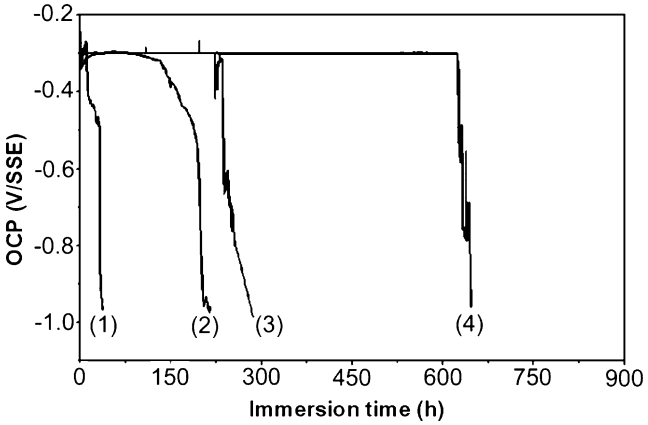

Fig. 3 Open-circuit potential (*OCP*) vs immersion time (h) in 3% NaCl solutions for PPy film electrodeposited on iron samples. Solutions for electrosynthesis: *1* pyrrole (0.1 M)+PTO (0.05 M); *2* pyrrole (0.1 M)+PTO (0.05 M)+DS (10^{-4} M)+α-Fe_2O_3; *3* pyrrole (0.1 M)+PTO (0.05 M)+DS (10^{-4} M)+Fe_3O_4; *4* pyrrole (0.1 M)+PTO (0.05 M)+DS (10^{-4} M)+γ-Fe_2O_3

achieving both passivity on iron and electrosynthesis of PPy on the resulting oxide film.

When DS is substituted to PTO as doping anion, the resulting morphology and current images show the aspect depicted as an example in Fig. 5a. Though the morphology looks very similar to that of the film grown with PTO, the conductivity (middle image) is significantly higher and, in this study again, there is no obvious correlation between the two images.

Figure 5b–d shows the influence of the different oxides when both PTO and DS anions are present. In this study again, the morphology does not significantly differ from those observed in Figs. 4a and 5a (top image). The conductivity is higher than that with PTO only but lower than that in the presence of DS only. The superficial conductivity of composite films containing Fe_3O_4 (see Fig. 5d) is better as compared with the one of films containing α- or γ-Fe_2O_3 nanoparticles (see Fig. 5b–c). It must be borne in mind that the particle concentration in the film is substantially higher with magnetite, and this must affect the resulting conductivity mapping. Finally, for the three samples (b to d), the distribution between the more and less conductive areas reveals a structure finer than in Fig. 5a or Fig. 4b. Indeed, it appears that average characteristic dimensions of conducting or insulating zones vary from 70 to 150 nm in Fig. 5b–d. The smallest zones in average are observed for PPy films containing α-Fe_2O_3 nanoparticles (see Fig. 5b), while the widest zones are observed in the presence of the two other oxides. Conductivity and morphology imaging for these oxides visually reveals some spatial correlations where the peaks appear to be more conductive than the valleys.

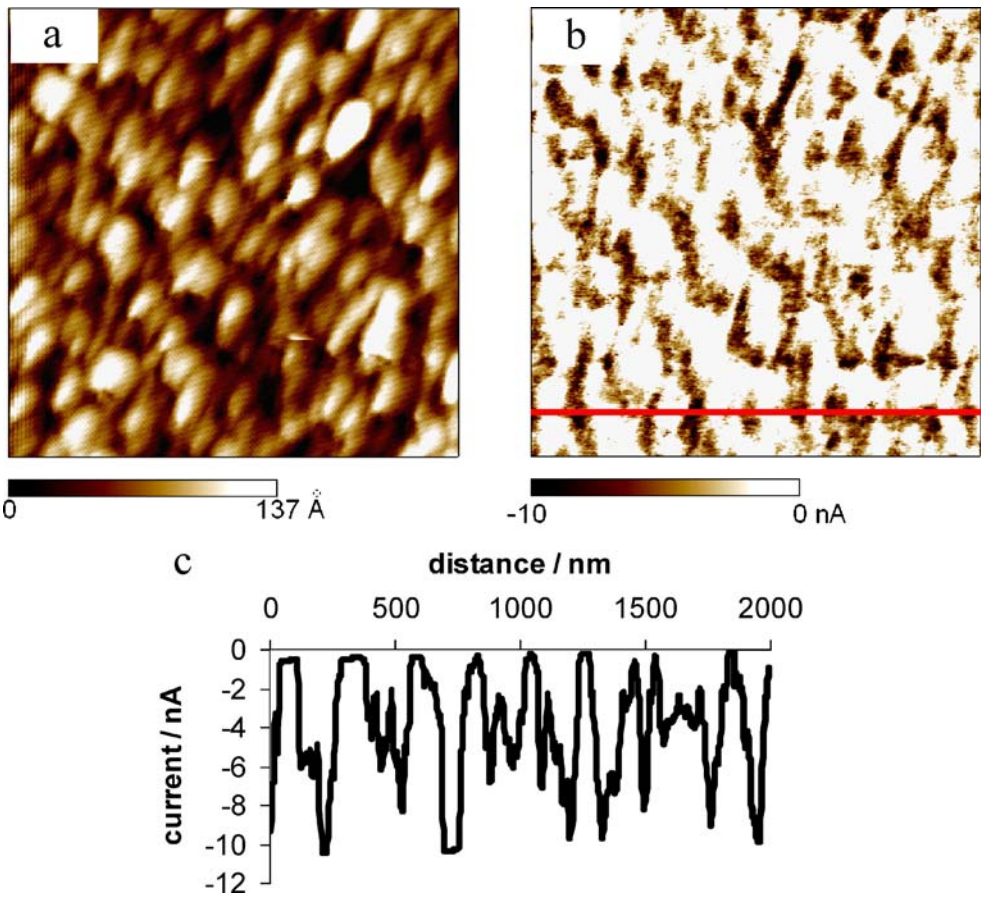

Fig. 4 Simultaneously recorded morphology (**a**) and current-sensing (**b**) AFM images of as-grown PPy films in water solution containing Py (0.1 M) and PTO (0.05 M). **c** Cross-sectional analysis of the current distribution. The bias voltage between the platinum substrate and the tip was −0.038 V, and the scanned area was 2×2 μm

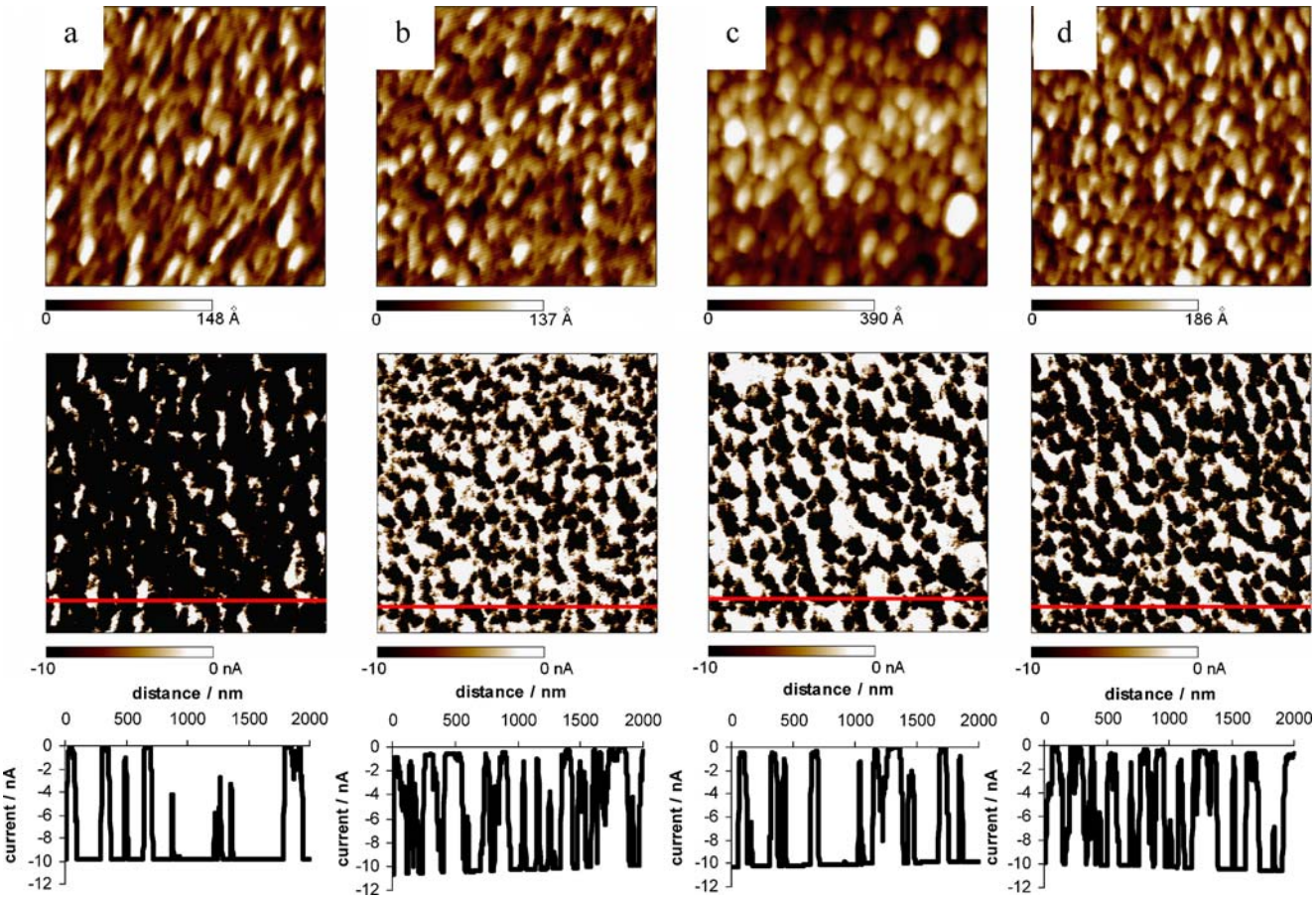

Fig. 5 Simultaneously recorded morphology (*top*) and current-sensing (*middle*) AFM images of as-grown PPy films in water solutions containing Py (0.1 M). **a** DS (10^{-4} M). **b** α-Fe_2O_3. **c** γ-Fe_2O_3. **d** Fe_3O_4. **b**–**d** Solutions contain also PTO (0.05 M) and DS (10^{-4} M). The *bottom figures* give examples of cross-sectional analyses of the current distribution. The bias voltage between the platinum substrate and the tip was −0.038 V, and the scanned area was 2×2 μm

In the absence of DS (Fig. 6a–c), the morphology is quite different with bigger bumps (200~300 nm) emerging from larger smoother areas. The conductivity is lower in particular in these smoother areas, and the bigger black features appear to be more conductive. The correlation between morphology and conductivity is clearer in this study.

Current–potential curves have been recorded by setting the tip in contact with the film at positions selected randomly and measuring the current for different bias potentials. Due to the characteristics of the AFM nose used in this work, the saturated current was ±10 nA.

As an example, the curves in Fig. 7 have been obtained with γ-Fe_2O_3 (conditions of Fig. 6a). Figure 7a–d is characteristic of conducting areas. Figure 7e corresponds to a poorly conducting area. Due to an uncompensated offset of the bias potential around −18 mV, zero current does not correspond to zero applied bias. When the curves are corrected from this artifact, they appear symmetrical as expected. In addition, the curves in Fig. 7a–d are purely ohmic as for good or metallic conductors. Conversely, the curve in Fig. 7e has a sigmoid shape which is rather encountered for semiconductors.

Discussion

A first and unexpected result is the much better conductivity of the film grown with DS only as compared to the film grown with PTO only. This could be an additional reason to explain why DS gives good performance with respect to corrosion protection as shown in the paper of Hien et al. [18]: it was in fact suggested that the PPy film which is p-doped behaves usually as an anionic exchange membrane; and when the synthesis is performed with large-size anions, these remain trapped after synthesis, and the film is only able to exchange cations, which prevents the ingress of anions such as chloride and therefore extends the lifetime of the film as a protective coating.

The other interesting result is that DS anions seem to promote a good dispersion of nanoparticles as the distribution is more even when it is present (compare Figs. 5 and 6).

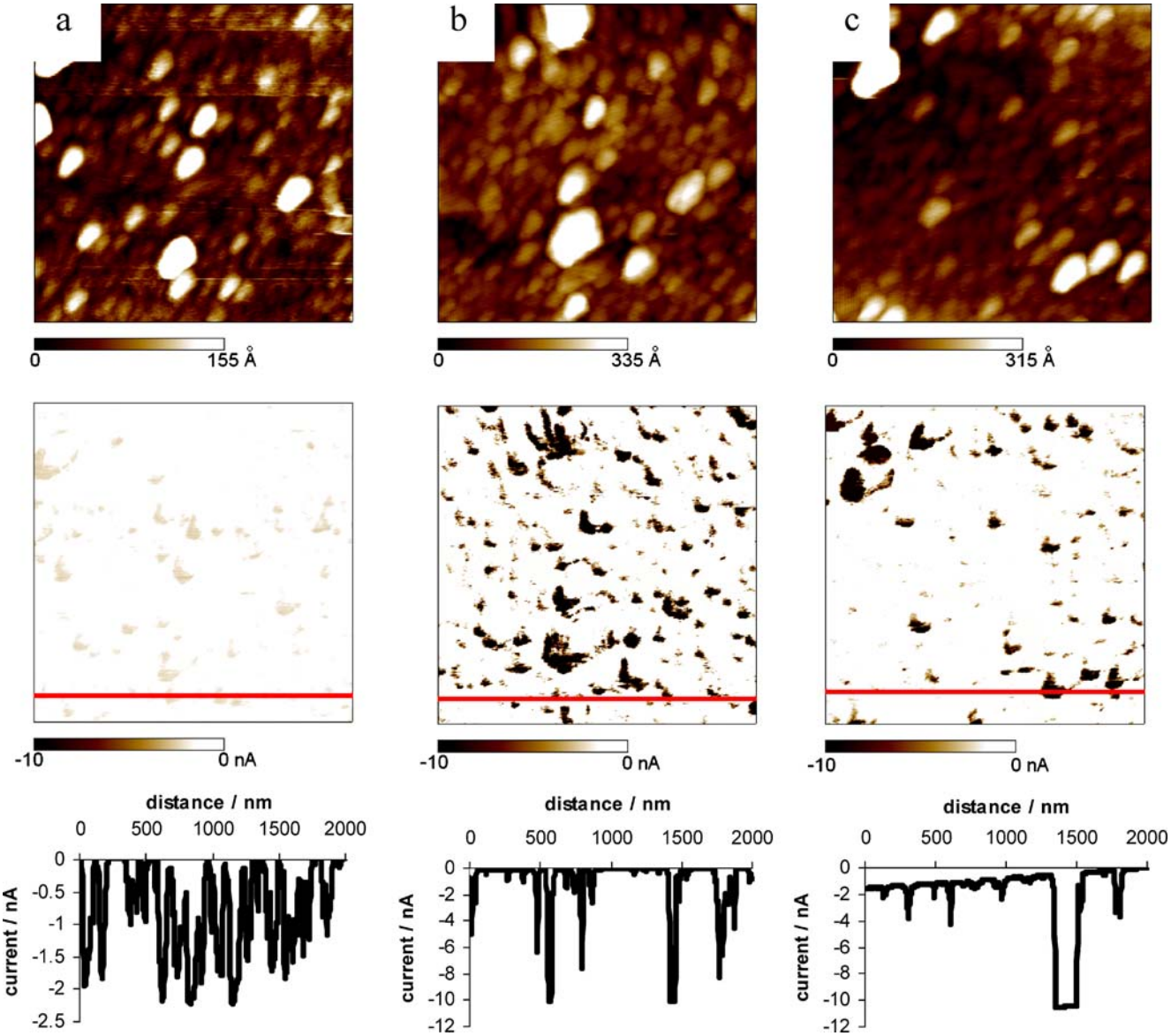

Fig. 6 Same imaging procedure as in Fig. 5. **a** Py (0.1 M), PTO (0.05 M), γ-Fe_2O_3. **b** Py (0.1 M), PTO (0.05 M), α-Fe_2O_3. **c** Py (0.1 M), PTO (0.05 M), Fe_3O_4. For the sake of comparison, the three CS-AFM images are displayed in this figure using the same current scale although it clearly appears that the chosen scale is not optimized for the CS-AFM of subpanel **a** where the current values are much lower than on the other CS-AFM images

However, the characteristic sizes of the small bumps are larger than the sizes of the nanoparticles. It cannot be argued that there is a single particle below each bump because the percentage of nanoparticles in volume would be too low as compared to the values given in Table 1. It must thus be considered that the particles are not completely separated and that there certainly remain clusters.

Concerning the correlation which seems to exist between morphology and conductivity (Figs. 5 and 6 in particular), one may put forward several explanations:

1. The protrusions correspond to parts of the film which grow faster and which could be accordingly associated to higher local conductivity. This would be consistent with a kinetic control of the growth by activation and not by diffusion because this last kinetics does not require a distribution of the surface conductivity but only a preexisting roughness which leads to a fractal growth (diffusion-limited aggregation process). In this case, the rms roughness would increase with the charge used for the synthesis. This point has not been checked in the present work, but it would deserve some attention in the future.
2. As there are particles continuously embedded in the film during the growth, one must admit that some of

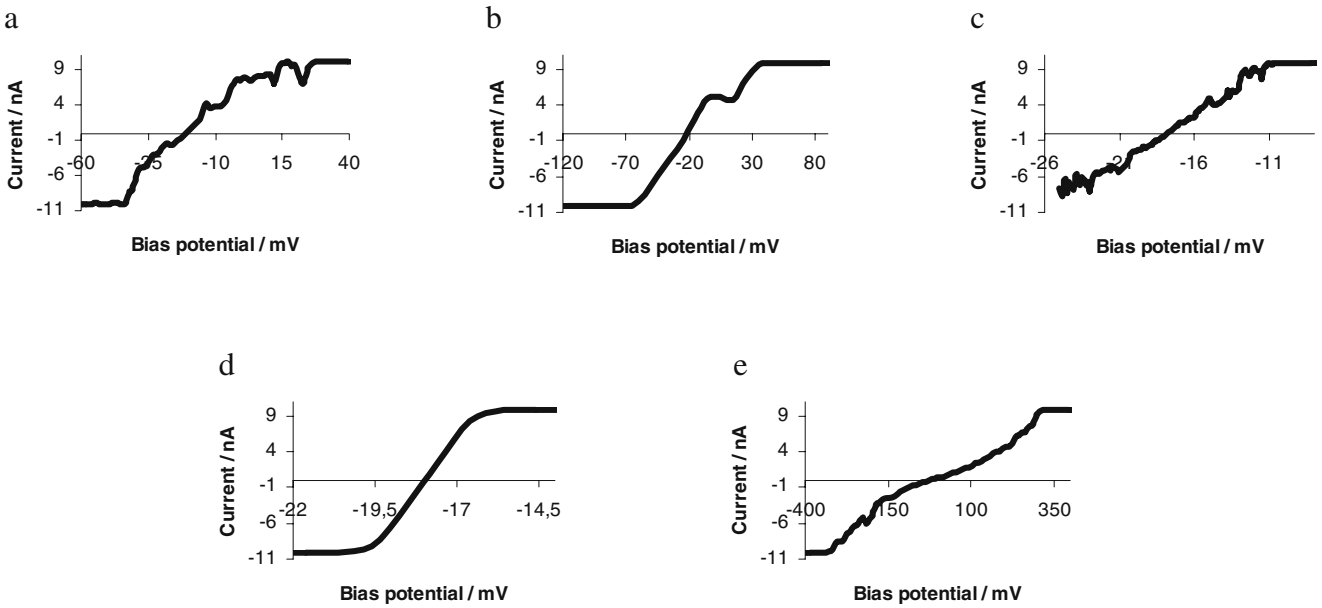

Fig. 7 Current potential curves for PPy films containing γ-Fe_2O_3 nanoparticles plotted at different spots of the sample (conditions of Fig. 6a) when the bias potential between the substrate and the conducting tip is varied symmetrically around zero

them have not yet started to be coated with PPy and in particular when the film growth is stopped. These spots could be areas of higher conductivity with respect to the surrounding areas corresponding to PPy. This explanation holds only for magnetite whose conductivity is in the order of a few hundreds of siemens per centimeter but not for maghemite or hematite that has a much lower conductivity than magnetite.

3. As said above, below the protrusions, one can suggest that there are individual particles or rather clusters. In this study, two scenarios can be invoked:
   - One could imagine that when the particles are embedded in the film, they act as seeds for subsequent growth of PPy as it has been shown that, in particular, the magnetite surface is an improved surface for the PPy growth [3]. The growth around and close to the nanoparticles would proceed in a more organized way, possibly in an epitaxial way as demonstrated earlier by Martin et al. [19, 20] for the "template synthesis" of PPy in microporous polycarbonate filters. Therefore, the conductivity on bumps would be higher by assuming a similar mechanism for oxide nanoparticles/PPy composites.
   - This growth of PPy on the nanoparticles could also occur in a solution by a chemical process due to their oxidative power. This actually occurs in a fast and spontaneous way with other oxides such as V_2O_5. The chemical synthesis could also proceed in an epitaxial way because these nanoparticles are single crystals and then they would be incorporated in the growing film. While there have been some models proposed to describe the mechanisms at the origin of the elaboration of metal/particle (insulating or conducting) composites, such models, to our knowledge, are not yet available.
4. It has been also suggested that the correlation between the morphology and the conductivity and notably the fact that protrusions are more conductive could be due both to the dynamic exploration of the surface by the tip and by the soft nature of the film. In this case, once the tip meets a protrusion, it makes locally a larger print and, therefore, the contact area between the tip and the film may increase. In fact, the expression of the contact resistance is defined either from the Maxwell resistance expression:

$$R_M = \rho/2\alpha$$

where ρ is the local resistivity of the material and α is the radius of the contact area assumed as a disk, or from the Sharvin resistance expression:

$$R_S = 4\rho\lambda/3\pi\alpha^2$$

where λ is the mean free path of electrons. In both cases, an increase of α leads to a decrease of R, and the materials may appear artificially more conducting.

The actual expression of the contact resistance is still an open problem for such soft materials because the geometry of the contact is not really known. In this domain, a more extended study on the I–V curves as a function of the applied force would be helpful in the future.

Conclusion

Composites elaborated from the electrosynthesis of PPy films in solutions containing nanoparticles of iron oxides have been investigated as good candidates for protection against corrosion of iron and carbon steel materials. Corrosion tests have shown that among magnetite, hematite, and maghemite moieties, maghemite offers the best performances.

A surfactant, the DS, was used to avoid the formation of clusters so as to improve the contact area between the nanoparticles and PPy. The effect of DS was shown to promote the clusters breaking and to substantially increase the film conductivity. The apparent correlation between the morphology and the local conductivity still needs further investigation.

References

1. Nguyen Thi Le H, Garcia B, Le Xuan Q, Deslouis C (2001) Electrochim Acta 46:4259
2. Nguyen Thi Le H, Garcia B, Le Xuan Q, Deslouis C (2002) J Appl Electrochem 32:105
3. Garcia B, Lamzoudi A, Pillier F, Nguyen Thi Le H, Deslouis C (2002) J Electrochem Soc 149:B560
4. Lee HJ, Park S-M (2004) J Phys Chem B 108:1590
5. Lee HJ, Park S-M (2005) J Phys Chem B 109:13247
6. Han D-H, Lee HJ, Park S-M, Parks GA (2005) Electrochim Acta 50:3085
7. Han D-H, Kim J-W, Park S-M (2006) J Phys Chem B 110:14874
8. Lee HJ, Park S-M (2004) J Phys Chem B 108:16365
9. Hong S-Y, Park S-M (2005) J Phys Chem B 109:9305
10. Han D-H, Park S-M (2004) J Phys Chem B 108:13921
11. Chang S-S, Wu C-G (2005) J Phys Chem B 109:18275
12. Planès J, Houzé F, Chrétien P, Schneegans O (2001) Appl Phys Lett 79:2993
13. Colley AL, Williams CG, D'Haenens Johansson U, Newton ME, Unwin PR, Wilson NR, Macpherson JV (2006) Anal Chem 78:2539
14. Wilson NR, Clewes SL, Newton ME, Unwin PR, Macpherson JV (2006) J Phys Chem B 110:5639
15. Holt KB, Bard AJ, Show Y, Swain GM (2004) J Phys Chem B 108:15117
16. Krstajić NV, Grgur BN, Jovanović SM, Vojnović MV (1997) Electrochim Acta 42:1685
17. Parks GA (1965) Chem Rev 65:177
18. Hien NTL, Garcia B, Pailleret A, Deslouis C (2005) Electrochim Acta 50:1747
19. Martin CR, Van Dyke LS, Cai Z (1992) Electrochim Acta 37:1611
20. Martin CR, Parthasarathy R, Menon V (1994) Electrochim Acta 39:1309